

Digital Simulation for Electrochemical Processes.

The Sherlock Holmes Magnifying Glass.

Maria Amélia Lemos

Centro de Química Estrutural, Instituto Superior Técnico, Av. Rovisco Pais 1, 1096
Lisboa Codex

Abstract

In this paper, the use of digital simulation as a tool to understand electrochemical data is discussed. The various approaches to digital simulation of electrochemical processes will be reviewed, and some applications of these methods to the interpretation of experimental results are presented.

Introduction

Science has always been supported on models that can be used to explain the reality. It is uncertain whether or not we can reach the truth behind what we observed in nature, but nevertheless we can construct models that do behave *approximately* like reality. As science evolves, the models tend to be more and more complex so that they are able to explain an increasing number of details of the observations. This complexity can assume many expressions and, often, it is not associated with the number and internal complexity of the equations describing the models, but more so on the complexity of the methods needed to solve apparently simple model equations. Simple and elegant models sometimes are quite troublesome to apply to real world problems, needing an immense amount of computational work.

The development of the personal computers has had a dramatic influence in solving real-world problems. The continuous increase in the power of desktop computers, giving them the performance that some years ago was only available in mainstream computers, have opened the possibility for the experimental chemist to have accessibility, at the workbench, to a wide range of computational capabilities to help in the solution of the problems encountered.

Electrochemical experiments have a long tradition of the use of digital simulation techniques to help in the understanding of mechanisms and on the estimation of parameters. Pioneering work has been published by Nicholson and Shain [1-4] and Feldberg [5,6] and since then a lot of development has been made, but only recently
Plenary lecture presented at the VII Meeting of the Portuguese Electrochemical Society -
III Iberian Meeting of Electrochemistry, Algarve, Portugal (1995)

the possibility of applying the methods has come to the personal computers and out of the big mainframe computers.

In this paper I wish to emphasise the possibilities opened to the experimental electrochemists, including synthetic chemists who use electrochemistry as a way of studying and characterising the compounds, by the use of these techniques. Much like *Sherlock Holmes' magnifying glass*, that helped the great detective to discover the clues to unfold the mystery, digital simulation allows the understanding of the processes occurring inside an electrochemical cell.

I will begin by presenting a brief summary of the main numerical methods available in literature to be used in digital simulation techniques for electrochemical processes in particular for cyclic voltammetry. A special attention will be given to the Method of Lines because it is the one chosen to perform the simulations shown here.

Finally I will also show how these methods can be applied to the study of coordination compounds, and present several examples of mechanisms that have been analysed by resorting to digital simulation techniques.

Background

To begin with, we will take a closer look at the problem at hand, what one expects to happen in the electrochemical cell during a dynamic experiment, and how modern science describes these problems and tackles with its solution.

During the investigation of the electrochemical behaviour of compounds in solution, more or less complex patterns are observed. This complexity arises partially from the nature of most of the electrochemical experiments, which can be described as perturbation-response techniques with a great amount of information in a single experiment. It would be desirable to be able to interpret the observed patterns in terms of a collection of electrochemical and chemical steps providing the researcher with an insight of the processes involved.

Let's consider what happens when an electrochemical experiment takes place. At a microscopic level the individual molecules of the electroactive species approach the electrode, giving it or receiving from it one or more electrons, and then move away from the electrode, possibly rearranging and/or reacting either intramolecularly or with other species present in solution. At a macroscopic level this results in the generation

of a concentration gradient, not only for the electroactive species, but also for all the other species that has a chemical interaction with them.

This concentration gradient that develops during the interaction of the species with the electrodes, constitutes the driving force that constantly moves molecules towards or away from the electrode.

This problem can be handled in the same way as most of the physical problems that are encountered. Modern science uses mathematical tools to model physical reality. These mathematical models, in particular in the case of dynamic systems, involves a set of differential equations that has to be solved so that we can predict future situations based on the knowledge of a particular (present) situation.

In this context, to obtain a profound understanding of the physical and chemical phenomena under study, we must always resort to these fundamental equations describing the work at hand. Unfortunately, the equations describing the coupled electron transfer and diffusion-reaction problems, involved in an electrochemical experiment are often hard to deal with, originating rather complex equations, most of which do not have an analytical solution, forcing us to resort to numerical methods in order to study these phenomena.

In this paper only cyclic voltammetry is considered but the basic concepts can easily be transferred to other types of dynamic experiments in stationary solutions, that is, in cases where diffusion is the main transport process.

Physical Description

Let us examine the way in which a typical cyclic voltammetry experiment progresses, considering the reduction of single species:



At the beginning of the scan, the current is virtually null and the concentration of the species is independent of the distance from the electrode (maximum concentration for the oxidised species and zero for the reduced one), as depicted in figure 1a. As the potential approaches the formal potential for the given redox pair, the oxidised species starts to be reduced at the electrode, generating the reduced species. This induces a gradient in the oxidised species that drives new molecules towards the electrode, whilst

for the reduced species, the gradient, produced by the generation of molecules at the electrode, drives molecules away from it. This is the situation depicted in figure 1b.

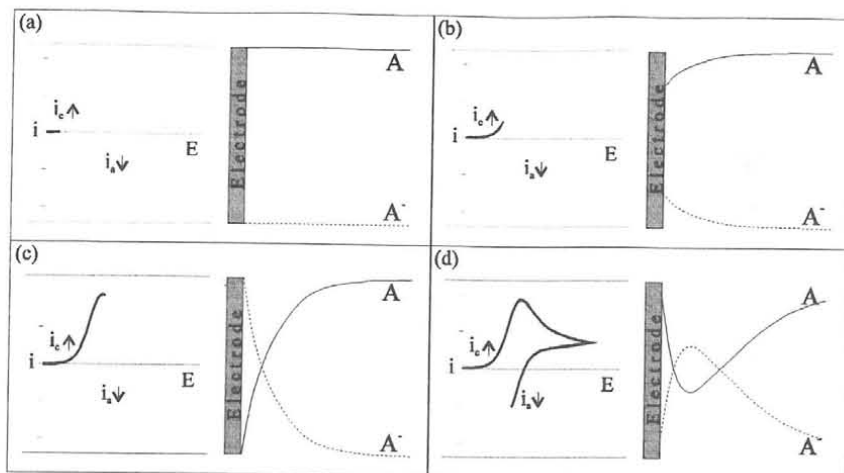


Figure 1 - Different stages in a cyclic voltammetry experiment.

The interconversion of the oxidised and reduced species at the electrode is responsible for the current that crosses the electrode and that is observed in our experiment.

During the first stages of the wave the process is mainly regulated by kinetic factors, but as the reactant is depleted near the electrode and new species must be transported, the process becomes diffusion controlled, as it is the case depicted in figure 1c.

A similar process occurs in the reverse sweep, but with the generation of the oxidised species and the consumption of the reduced one (fig. 1d).

Mathematical Description

Lets first look at the general mathematical description for an electrochemical process occurring at a stationary electrode.

In a stationary electrode, when a potential is applied it generates a gradient of the concentration of the electroactive species.

If the solution is divided into equally spaced intervals, which can be considered as small slabs, in the case of a planar electrode, with a thickness Δx , the concentration

computers without an enormous *amount of memory* and it is fairly *easy to code* in a program, and there is no need of a profound *mathematics knowledge* to implement it. Also, this method is also relatively simple to adapt to new mechanisms.

With some adjustments, as demonstrated below, it can maintain a good accuracy even with rather high kinetic constants, and it is stable for a large set of conditions.

Method of Lines

In the method of lines, has stated above, a semi-discretisation is performed. That is, the differential equations describing the process are discretised only in relation to the spatial coordinates.

This leads to a set of ordinary differential equations, describing the way the concentration of the different species vary with time at each of the space points considered.

Going back to the development of the second Fick's law, this is much like considering the mathematical description of the process with finite space intervals, just before we take the limit to an infinitesimal space element.

The set of ordinary differential equation can be then integrated using one of the many methods available, like the Euler method, the Runge-Kutta methods or multi-step predictor corrector methods [44, 45].

In a first approach we might think that it would be simpler to divide the space coordinates in an evenly space grid. However, the problem we are trying to solve has some general and particular characteristics of its own.

Most of the *events* occur relatively near the electrode. It is at the electrode that the electroactive species are generated or consumed, and, in the case of subsequent chemical reactions, the electrode is, in fact, the starting point of these reactions, which are induced by the electron transfer processes.

It is, then, advisable to divide the space coordinates into unevenly spaced elements. These elements are closer to each other near the electrode, where the concentration changes sharply with position, and are wider apart far from the electrode, where the concentration profile is almost flat.

This physical reasoning is related to a mathematical reason also. If we consider the solution divided into sections, we should take them so that the concentration can be

considered as *approximately* constant for each element. So the width of an element should be smaller near the electrode than far.

The formula used to compute the spacing of the points usually involves an exponential increase in this spacing [8,9], like in the expression below.

$$\Delta x_i = \Delta x_0 e^{\beta i}$$

In this equation, Δx_0 is the width of the first space element, and β is the expansion coefficient. The larger the value of β , the more the spacing between the elements increase as we move away from the electrode.

The importance of the adequate choice of the space grid that is used has been demonstrated using a fixed integration method, the fourth-order Runge-Kutta, and examining how the error changed with the space discretisation procedure [27]. The error was computed comparing the simulated voltammograms with the theoretical one (for an infinite diffusion layer) published by Nicholson and Shain [1].

This is represented in figure 3.

Several parameters have to be taken into account. They are:

- the total width of diffusion layer considered - *i.e.* the distance into the solution where we are going to compute the concentration changes;
- the number of intervals considered, *i.e.* the number of intervals into which the diffusion layer is going to be subdivided;
- the expansion parameter, *i.e.*, the unequal subdivisions being made to the diffusion layer under consideration.

Of course, it is clear that the more intervals considered, all other things remaining constant, the more accurate will our description of the events be, but also the more computational time will be required. All these three parameters will have to be balanced in order to have an accurate simulation with the least computational effort and time.

One of the most important parameters to consider, of course, is the correctness of the diffusion layer thickness, which can be estimated according to methods in the literature [24]. If the diffusion layer thickness is correct, then the error can assume acceptable levels even for a small number of space elements, if the value for β is well chosen. If the diffusion layer considered is too large, computations will be made in relation to areas of the solution that are unaffected by the experiment being carried

out. If the diffusion layer is too small, a considerable distortion will occur in the voltammogram.

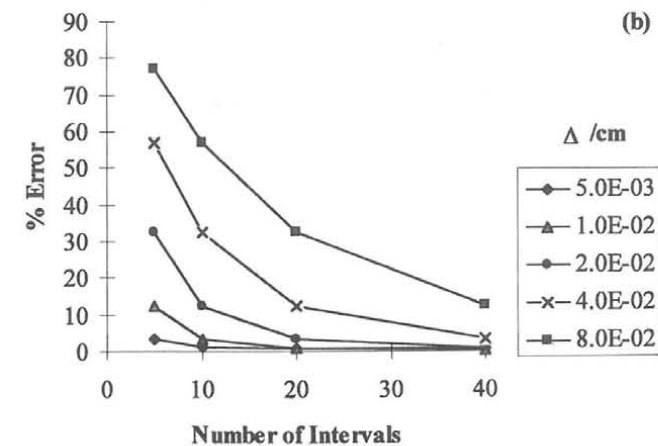
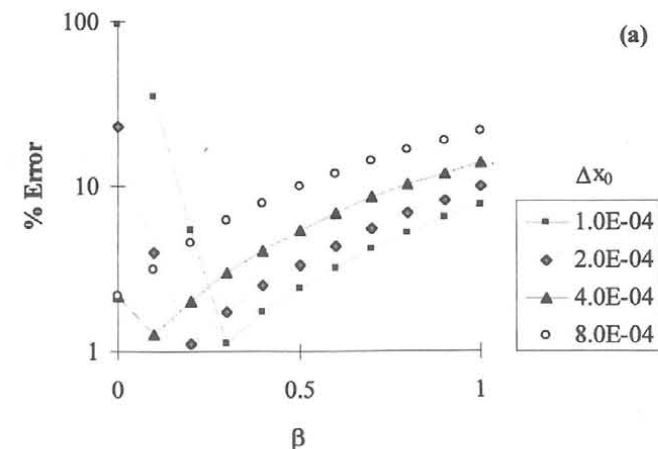


Figure 3 - (a) Representation of the error as a function of the expansion parameter (β) and of the width of the interval closer to the electrode (Δx_0), for a fixed number of intervals. (b) Representation of the error as a function of the total number of intervals for a fixed diffusion layer thickness (Δ) and $\beta = 0$. Simulations were done for a simple E mechanism [27].

The use of unequal intervals also allows for the use of fewer intervals, by concentrating these intervals in the regions where they are needed the most to describe all the changes in the concentration profiles, that happen near the electrode.

A main conclusion can be drawn. By using an adequate space discretisation technique, carefully choosing both the width of the diffusion layer and the expansion parameter, it is possible to perform accurate simulations using very few space intervals and, thus, with a very limited computational effort.

However, space discretisation is not the only important factor.

It is known that the methods available for the solution of ordinary differential equations have very large differences, both in error levels attained and in the performance and computational weight they require.

In the following we will analyse the influence of the numerical method used to integrate the ordinary differential equations obtained by the semi-discretisation procedure, analysing it both on the viewpoint of accuracy and computational speed [26].

The analyses is made using the ECECE mechanism depicted in figure 4, that will be used in the discussion of the applications of this procedure to experimental data, and which contains several electron-transfer steps coupled with homogeneous chemical reactions, thus providing a rather complex mechanism that allows us test our methods in a real-world situation.

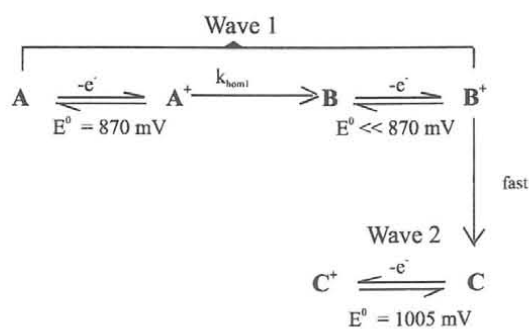


Figure 4 - ECECE mechanism considered in this work, with the standard redox potentials (E^0) used in the simulated voltammograms.

The methods considered were Euler, modified Euler (equivalent to second order Runge-Kutta), third and fourth order Runge-Kutta and the Adams-Moulton and Milne multi-step predictor-corrector methods [44]. Space discretisation was carried out using an evenly spaced grid so that the only influence in the error results is the time integration method.

The Milne method proved to be entirely unsuitable due to a severe lack of stability in most of the situations encountered.

The study was conducted by computing the errors obtained when both the scan rate and the rate constant for the first chemical step were varied.

Figure 5 depicts the error of the simulations as a function of these two parameters. As it can be easily seen, the numerical method, the Euler method in this case, is unable to cope with large kinetic rate constants when simulating slow scan rates. All the simulations in this graph were performed with a 1 mV integration step. Better results would be obtained with smaller steps, but at the expense of increasing the computation time.

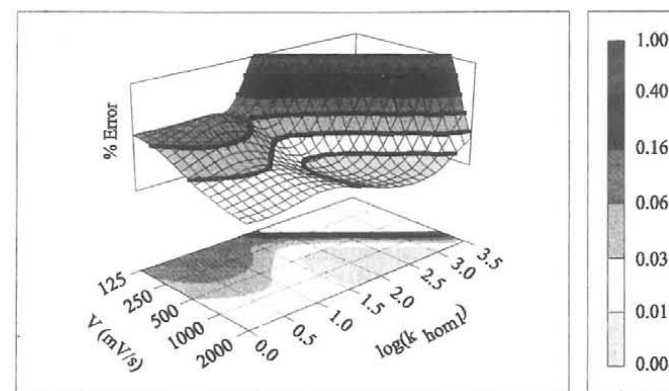


Figure 5 - Surface representing the average error (%) as a function of the scan rate (log scale) and the logarithm of the homogeneous rate constant k_{hom1} obtained for the Euler method with a 1 mV step size.

In figure 6, representing a projection of the curve shown previously, we can see that if one uses a better integration procedure, one is allowed to use the method in a wider range of conditions.

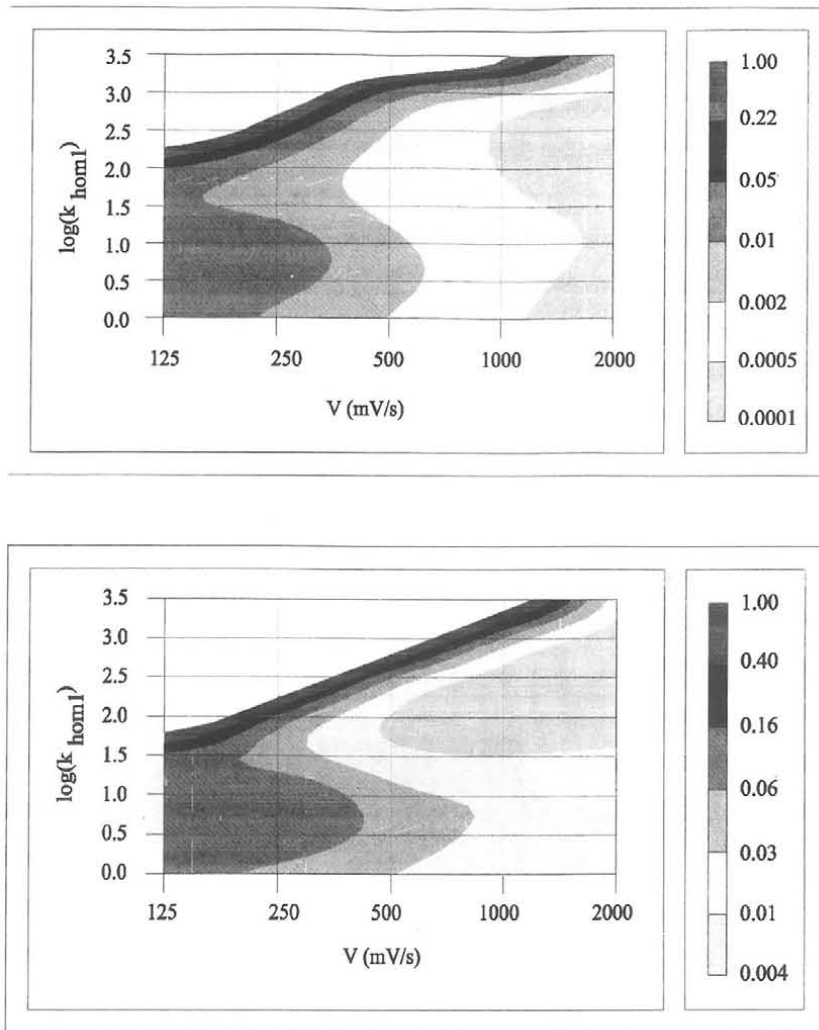


Figure 6 - Average error regions (%) for the modified Euler (a) and fourth order Runge-Kutta (b). Areas indicated as having 1% error correspond to unstable regions.

Observing the area where the Euler method was unable to produce adequate results, the upper left corner in the graph, and comparing it with the same projection for the fourth-order Runge-Kutta method, it can be seen that the latter has a much wider stability area.

But the error level is just one of the factors that have to be taken into consideration. Theoretically if we performed computations with a very small step, as well as a very close space grid, we would obtain arbitrarily accurate results. The price we would have to pay for this would be to wait forever to see the results.

Let us then consider this comparison in terms of the error obtained as a function of the computation time. We can see in figure 7 that, for a given computational time, the method that produces the least error is the Adams-Moulton, followed by the fourth-order Runge-Kutta method, and then the Euler method. Amazingly the third order Runge-Kutta produced always worse results than the modified Euler (which is the same as the second-order Runge-Kutta) did, although it had a larger stability area.

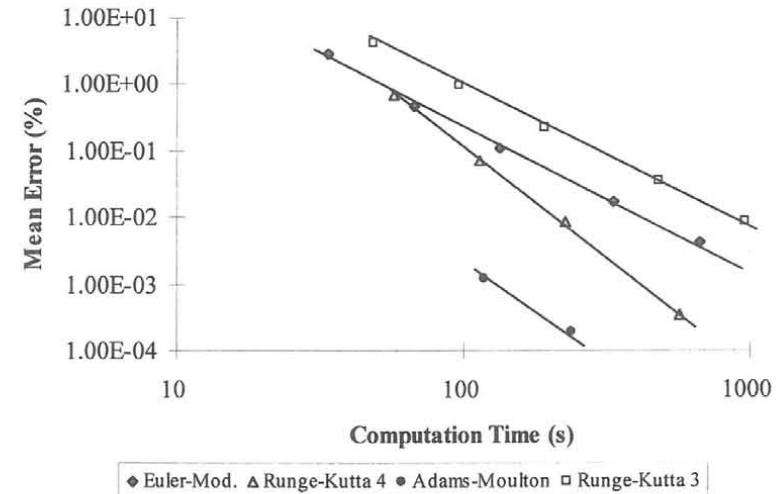


Figure 7 - Comparison of the average error versus computation time, for the modified Euler, 3rd and 4th order Runge-Kutta, and Adams-Moulton integration methods, applied to an ECECE scheme ($k = 10 \text{ s}^{-1}$, scan rate = 200 mV).

The Adams-Moulton method was amazingly accurate, giving errors several orders of magnitude below the fourth-order Runge-Kutta, but had a very small stability domain. It worked well when it worked, but it did not work very often.

Similar conclusions can be drawn in the slightly tougher situation depicted in figure 8. The homogeneous rate-constant is tenfold the previous one, but the scan rate is only fivefold.

The distinction of the error levels between the methods is less clear in this case and, sometimes, the modified Euler is even better than the fourth-order Runge-Kutta, that giving lower errors for the same computational time.

As a general conclusion it can be said that a program using an exponentially expanding space grid and either the modified Euler or the Fourth-order Runge-Kutta methods for the numerical integration of the ordinary differential equations, is a very adaptable and powerful tool to help in the study of electrochemical phenomena, giving computational times and error levels which are very acceptable, even on a small desktop microcomputer.

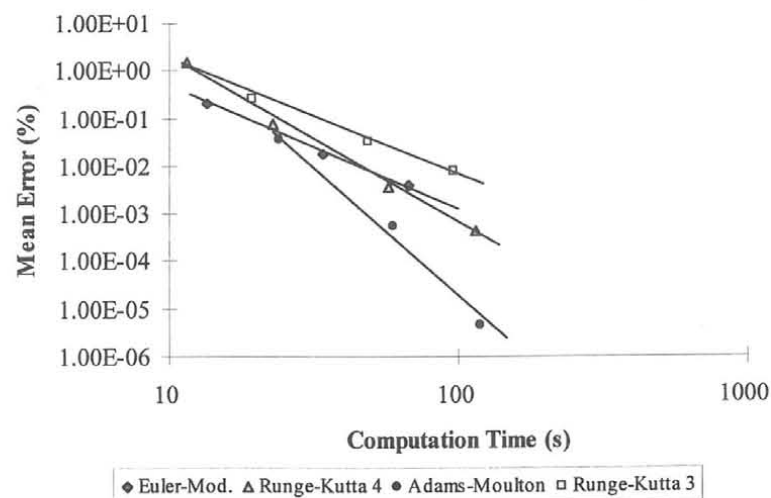


Figure 8 - Comparison of the average error versus computation time, for the modified Euler, 3rd and 4th order Runge-Kutta, and Adams-Moulton integration methods, applied to an ECECE scheme ($k = 100 \text{ s}^{-1}$, scan rate = 1000 mV).

Notice that the computational times are always below 100 seconds, less than two minutes for each simulation, with average error levels well below 0.1 %.

These simulations described above were carried out on a 386SX/25 MHz based IBM compatible personal computer with a fasmath Cyrix math coprocessor [26, 27]. The power of desktop computers has increased more than ten times since the 386SX machines, and still keeps increasing, giving us the ability to perform faster simulation and/or more complex ones.

Applications

In the following some applications of digital simulation to the study of coordination chemistry systems reactivity will be presented. The application of these techniques has allowed the enlightenment of some mechanistic aspects, as well as the evaluation of electrochemical and chemical parameters.

[FeH(CNR)(dppe)₂] [BF₄]

Let's begin with an interesting system of hydride complexes of iron II.

Although the work was carried out over a range of complexes with different R's [46], only the data concerning R = methyl is going to be discussed as an example.

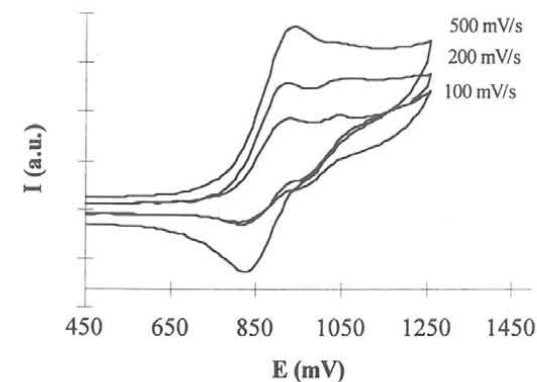


Figure 9 - Cyclic voltammograms for *trans*-[FeH(CNMe)(dppe)₂]⁺ at several scan rates, in 0.2 M [Bu₄N][BF₄]/thf.

These compounds show an anodic oxidation wave, at about 900 mV (*versus* S.C.E.), which is partially reversible. This reversibility decreases as the scan rate is decreasing and, below 100 mV/s, they show no cathodic counterpart. This wave is followed by a second oxidation wave, visible only at low scan rates. This wave is

reversible at the scan rate range that was studied. This behaviour can be seen in figure 9.

Figure 10-a shows the current-function for the first anodic wave at room temperature and at -30°C. There is a remarkable increase in the current-function for lower scan rates at room temperature, which is in agreement with an hypothesis of two electrons being exchanged at slow scan rates. The current-function at -30°C, however, is almost constant. At low temperatures wave I becomes reversible and the current-function is constant and consistent with one electron being exchanged.

In order to obtain more data about this process, we compared the current-functions for wave I in the presence and absence of pyridine. The ratio between the current-function with added pyridine and without pyridine was measured. This ratio increases, with increasing scan rate, to a value higher than unity, until about 100 mV/s, and then remains constant, as can be seen in figure 10-b.

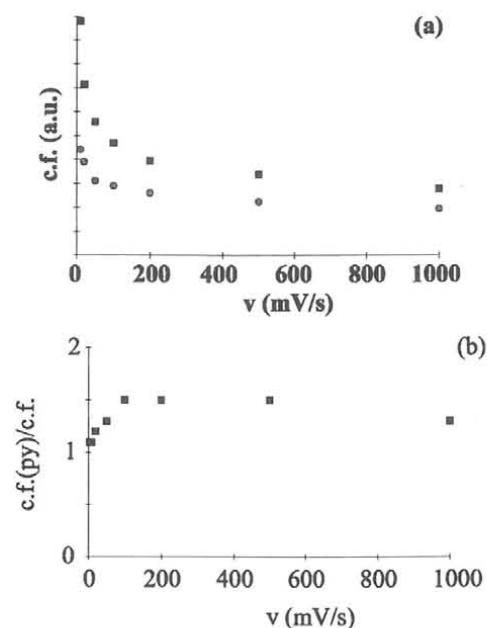


Figure 10 - (a) Current-function for the first anodic wave for the complex $trans-[FeH(CNMe)(dppe)_2]^+$ at room temperature (■) and -30 °C (○). (b) Ratio between the current-function with added pyridine and without pyridine (c.f.(py)/c.f.) at room temperature.

Pyridine is a base which would increase a possible deprotonation reaction rate, a reaction that is supposed to occur at wave I. This effect is more important when the deprotonation is the rate limiting step, that is, at high scan rates. At low scan rates the deprotonation reaction can proceed in full extension, and the addition of pyridine does not represent a significant increase in the global rate of the process and, thus, does not affect the current-function.

So we can imagine an ECE-type mechanism where, in the first step, an electron is transferred, giving a Fe(III) complex, which can easily lose its hydride as an H^+ . This is the reaction that could be speeded up with the addition of pyridine. The complex that is obtained has a low oxidation state (Fe(I)) and, at this potential, is readily oxidised to iron (II). Thus, E_2^0 is certainly lower than E_1^0 . This complex has a vacant coordination position and it can easily suffer a nucleophilic attack by the fluoride anion of the electrolyte, giving the fluoride iron(II) complex, which is oxidised, at the second wave. The global behaviour can then be described by an ECECE mechanism, as depicted in figure 11. This ECECE-type mechanism was then simulated in the computer to see how well it fitted the experimental data.

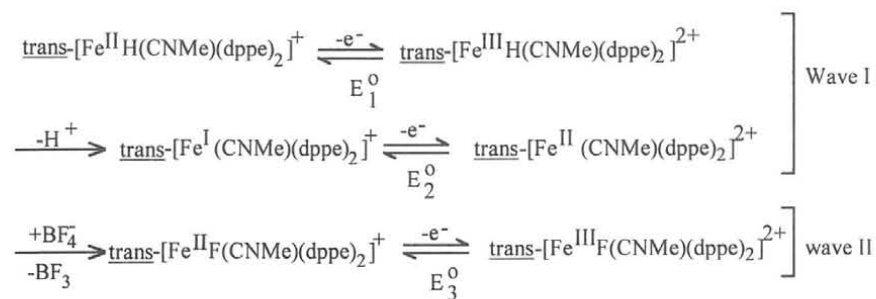


Figure 11 - Proposed ECECE-type mechanism for the anodic process of $trans-[FeH(CNMe)(dppe)_2]^+$ in 0.2 M $[Bu_4N][BF_4]/thf$.

In order to understand how each parameter changed the simulated voltammogram, the simulations are going to be presented step by step.

First let us examine the changes introduced to the voltammogram when the fluorination reaction rate constant, k_{hom2} , varies from $0 s^{-1}$ to infinity (figure 12(a)). The main effect is, as expected, the increase in the second oxidation wave's intensity, as we

increase $k_{\text{hom}2}$, (all other parameters were kept constant, with the protonation reaction rate constant, $k_{\text{hom}1}$, equal to 0.9 s^{-1}).

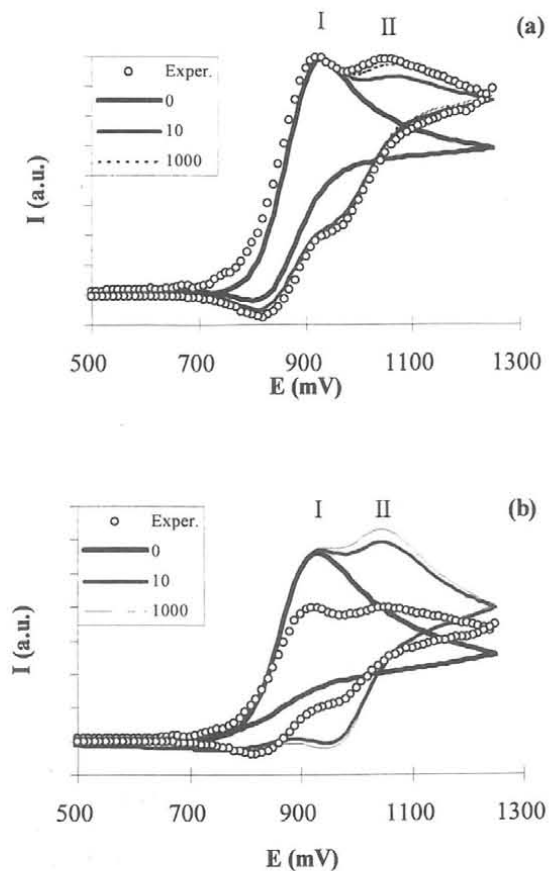


Figure 12 - Influence of fluorination reaction rate, $k_{\text{hom}2}$, varying from 0 s^{-1} to infinity, on the simulated voltammogram at 100 mVs^{-1} for an ECECE process when (a) $k_{\text{hom}1} = 0.9 \text{ s}^{-1}$ and (b) $k_{\text{hom}1} = 10 \text{ s}^{-1}$, for various values of $k_{\text{hom}2}$.

If we use a higher value for the deprotonation reaction rate (10 s^{-1} - figure 12(b)), the effect on the second oxidation wave is more important, accordingly to the increase in the production of the unsaturated iron (II) complex.

The fluorination reaction rate constant has no significant influence on the intensity of the first wave.

Next we will see the effect of the deprotonation reaction rate on the simulated voltammograms, which is depicted in figure 13.

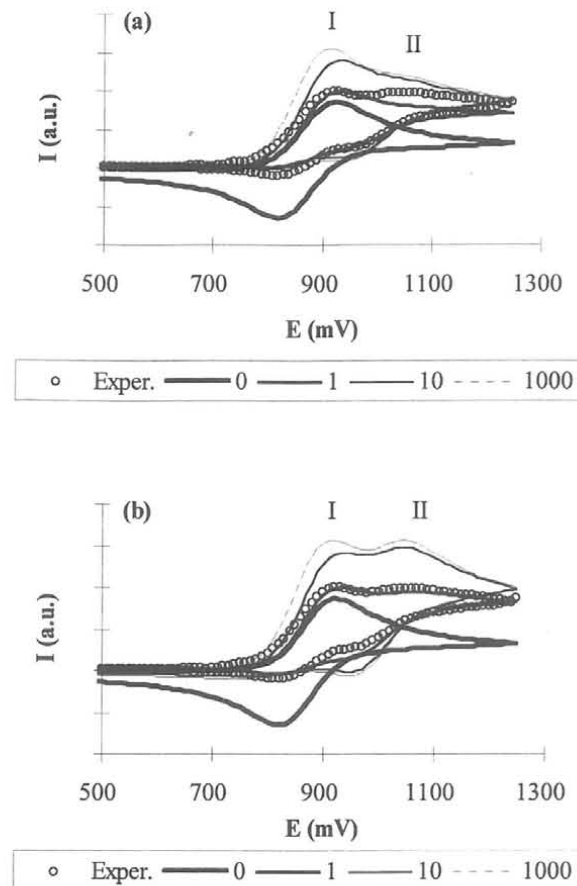


Figure 13 - Influence of the protonation reaction rate, $k_{\text{hom}1}$, on the simulated voltammogram at 100 mVs^{-1} for an ECECE process when (a) $k_{\text{hom}2} = 1.0 \text{ s}^{-1}$ and (b) $k_{\text{hom}2} = \text{infinity}$.

It can be clearly seen that an increase in the deprotonation rate constant leads to an increase of the intensity of the first oxidation wave, because more species is converted to the unstable iron(I) complex, which is readily oxidised at the potential for wave I. In the simulations in figure 13(a) the fluorination rate constant, $k_{\text{hom}2}$, was kept constant at 1.0 s^{-1} , whilst in figure 13(b) we can see the influence of $k_{\text{hom}1}$ for a very large value

of $k_{\text{hom}2}$. Since, in the latter case, the rate of fluorination is higher, the increase in $k_{\text{hom}1}$ induces a more pronounced increase in the intensity of the second oxidation wave.

In figure 14 the influence of the heterogeneous rate constant for the first electron transfer is shown.

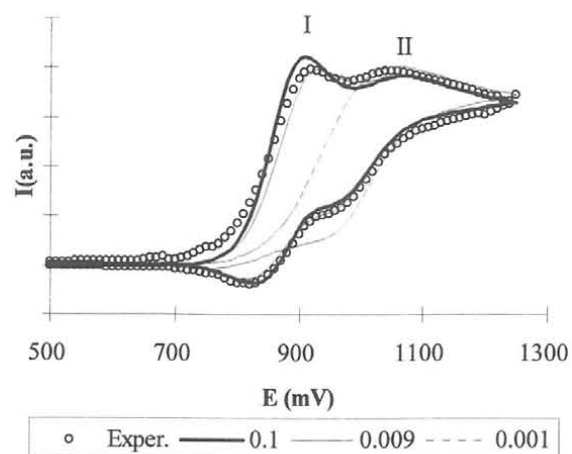


Figure 14 - Influence of the heterogeneous rate constant in a voltammogram simulated at 100 mV/s for the ECECE mechanism discussed in the text.

For electron-transfers that fall into the category of quasi-reversible processes, as it is the case of the processes under inspection, the shape of the voltammogram is strongly influenced by the value of the heterogeneous rate constant, as you can see in this graph.

A similar procedure can be used in all cases to estimate the electrochemical parameters of a particular redox process.

The complete process, which in fact takes quite a while in experimenting and changing all the relevant parameters for a particular model, leads us to the final results, which are represented, for two different scan rates, in figure 15. The final values we obtained fit experimental data quite well. The relevant data for a whole family of compounds has been obtained in this way [46].

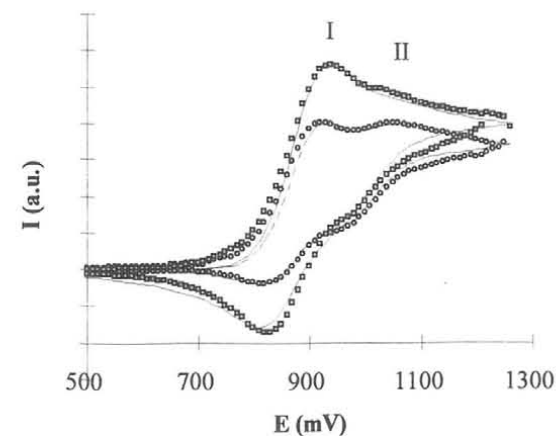


Figure 15 - Final fittings for the experimental voltammograms for $\text{trans-[FeH(CNMe)(dppe)}_2\text{][BF}_4\text{]}$ at 500 mV/s (■) and 200 mV/s (●).

$\text{trans-[ReCl(CNH}_2\text{)(dppe)}_2\text{][BF}_4\text{]}$ and $\text{trans-[ReCl(CNHMe)(dppe)}_2\text{][BF}_4\text{]}$

Another interesting mechanism involves rhenium aminocarbonyl complexes, and also the use of digital simulation played an important role in enlightening the chemical process under observation.

$\text{trans-[ReCl(CNHMe)(dppe)}_2\text{][BF}_4\text{]}$ presents a voltammogram showing a two electron oxidation, in thf, with a peak potential around 0.98 V (versus s.c.e.). The return cycle shows a clear reduction with a half-wave potential around 0.08 V (versus s.c.e), for which a reversal of the scan exhibits an anodic counter part, significantly larger than the small wave that was observed for these potentials at the beginning of the cycle [47, 48] (see figure 16).

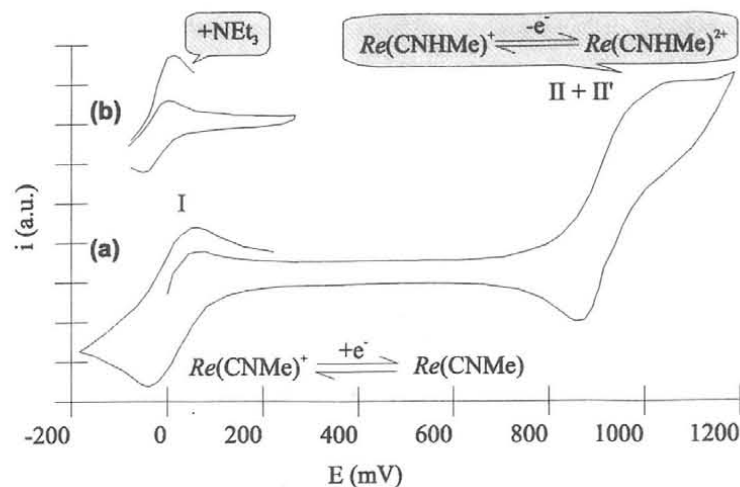


Figure 16 - (a) Cyclic voltammogram of *trans*-[ReCl(CNHMe₂)(dppe)₂][BF₄] in thf at 200 mVs⁻¹. (b) Observed increases in the oxidation peak intensity of wave I upon addition of a base. *Re* = {ReCl(dppe)₂}

This behaviour was interpreted according to the extended square scheme shown in figure 17.

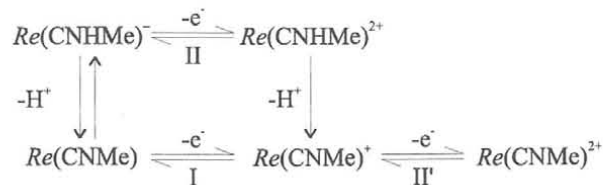


Figure 17 - Extended square scheme proposed for the electrochemical behaviour of *trans*-[ReCl(CNMe)(dppe)₂][BF₄] in thf. ECE mechanism for wave II(+II') confirmed with digital simulation. *Re* = {ReCl(dppe)₂}

The first electron-transfer also involves the loss of a proton by the aminocarbyne complex, leading to the isocyanide complex *trans*-[ReCl(CNMe)(dppe)₂]⁺, which is readily oxidised at this potential. These two electron-transfer processes, occurring in an ECE-type mechanism correspond to the two-electron wave at 0.98 V.

The reduction of the rhenium(II) isocyanide complex is responsible for the reduction wave that is observed on the reverse sweep. The small wave that can be seen

at the beginning of the cycle, with a potential that is compatible with the Re(I)/Re(II) isocyanide complex was attributed to an acid/base equilibrium between the *Re*(CNHMe)⁺ aminocarbyne and the *Re*(CNMe) isocyanide species (figure 17). This was confirmed by the addition of a base, which induced a sharp increase in the wave that is observed at around 0 V at the beginning of the cycle, as can be seen in figure 17(b).

The complete mechanism was simulated in the computer leading to the results shown in figure 18, where a very good agreement between the experimental and theoretical voltammograms is obtained.

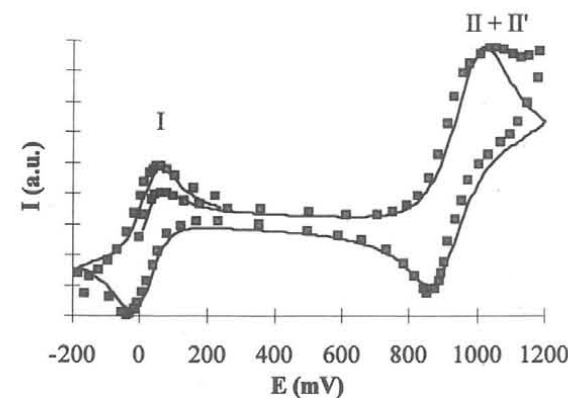


Figure 18 - Final fitting for the experimental voltammogram (■) of *trans*-[ReCl(CNHMe₂)(dppe)₂][BF₄] in thf at 200 mVs⁻¹.

A related mechanism which has been interpreted as a ladder scheme is the electrochemical behaviour shown in acetonitrile by the rhenium aminocarbyne *trans*-[ReCl(CNH₂)(dppe)₂][BF₄] [49].

In acetonitrile it shows a first oxidation wave around 1 V (*versus* s.c.e), with no cathodic counterpart at all the scan rates that were used. After this oxidation, and in a similar manner to the previous system, there is a proton loss leading to the corresponding isocyanide complex, which, in his turn, is oxidised at around 1.7 V (*versus* s.c.e.). The reduction of the rhenium (II) isocyanide is also observed at around 0.4 V (*versus* s.c.e.) as can be seen in figure 19. However, the rhenium (III) isocyanide

- [5] S.W. Feldberg, "Electroanalytical Chemistry - vol. 3", A.J. Bard (Ed), Marcel Dekker, 1969, New York.
- [6] S.W. Feldberg, C. Auerbach, *Anal. Chem.* 36 (1964) 505
- [7] S.W. Feldberg, C. Auerbach, *Anal. Chem.* 36 (1964) 505.
- [8] S.W. Feldberg, *J. Electroanal. Chem.*, 127 (1981) 1.
- [9] J. Joslin, D. Pletcher, *J. Electroanal. Chem.*, 49 (1974) 171.
- [10] R.D. Moulton, A.J. Bard, S.W. Feldberg, *J. Electroanal. Chem.*, 256 (1988) 291.
- [11] I. Ruzic, S.W. Feldberg, *J. Electroanal. Chem.*, 50 (1974) 153.
- [12] B. Marques da Silva, L.A. Avaca, E.R. Gonzales, *J. Electroanal. Chem.*, 269 (1989)1.
- [13] D. Britz, B. Marques da Silva, L. Avaca, E.R. Gonzales, *Anal. Chim. Acta*, 239 (1990) 87.
- [14] S.W. Feldberg, *J. Electroanal. Chem.*, 290 (1990) 49.
- [15] S.A. Lerke, D.H. Evans, S.W. Feldberg, *J. Electroanal. Chem.*, 296 (1990) 299.
- [16] G.L. Booman, D.T. Pence, *Anal. Chem.*, 37 (1965) 1366.
- [17] J. Heinze, M. Störzbach, J. Mortensen, *J. Electroanal. Chem.*, 165 (1984) 61.
- [18] D. Britz, J. Heinze, J. Mortensen, M. Störzbach, *J. Electroanal. Chem.*, 240 (1988) 27.
- [19] M. Rudolph, *J. Electroanal. Chem.*, 314 (1991) 13.
- [20] A.R. Gourlay, *J. Inst. Math. Appl.*, 6 (1970) 375.
- [21] D. Shoup, A. Szabo, *J. Electroanal. Chem.*, 160 (1984) 1.
- [22] D. Shoup, A. Szabo, *J. Electroanal. Chem.*, 199 (1986) 437.
- [23] S. Pons em "Electroanalytical Chemistry", Vol. 13, A.J. Bard (Ed.), Marcel Dekker, 1984, Nova York, p. 115.
- [24] Britz, D., "Digital Simulation in Electrochemistry", 2ª Ed., Springer Verlag, 1988, Berlin.
- [25] D. Britz, *J. Electroanal. Chem.*, 240 (1988) 17.
- [26] M. Amélia N.D.A. Lemos, A.J.L. Pombeiro, em A.J.L. Pombeiro et al (Eds.) "Molecular Electrochemistry of Inorganic, Bioinorganic and Organometallic Compounds", Kluwer Academic Publishers, NATO ASI series vol. 385, 1993, Dordrecht.
- [27] M. Amélia N.D.A. Lemos, A.J.L. Pombeiro, *Port. Electrochim. Acta*, 10 (1992) 89.

- [28] M. Amélia N.D.A. Lemos, A.J.L. Pombeiro, *J. Organomet. Chem.*, 438 (1992) 159.
- [29] R.S. Nicholson, M.L. Olmstead, em "Electrochemistry. Calculations, Simulation and Instrumentation", J.S. Mattson, H.B. Mark Jr., H.C. MacDonald Jr., Marcel Dekker, 1972, Nova York.
- [30] W.H. Reinmuth, *Anal. Chem.*, 34 (1962) 1446.
- [31] R.S. Nicholson, I. Shain, *Anal. Chem.*, 36 (1964) 706.
- [32] R.S. Nicholson, I. Shain, *Anal. Chem.*, 37 (1965) 178.
- [33] M. Rudolph, *J. Electroanal. Chem.*, 292 (1990) 1.
- [34] K.B. Oldham, *Anal. Chem.*, 58 (1986) 2296.
- [35] J. Leddy, *J. Electroanal. Chem.*, 300 (1991) 295.
- [36] L.F. Whiting, P.W. Carr, *J. Electroanal. Chem.*, 81 (1977) 1.
- [37] B. Speiser, A. Rieker, *J. Electroanal. Chem.*, 102 (1979) 1.
- [38] P. Hertl, B. Speiser, *J. Electroanal. Chem.*, 217 (1987) 225.
- [39] M.M. Stephens, E.D. Moorhead, *J. Electroanal. Chem.*, 220 (1987) 1.
- [40] E.D. Moorhead, M.M. Stephens, *J. Electroanal. Chem.*, 282 (1990) 1.
- [41] M. Penczek, Z. Stojek, J. Osteryoung, *J. Electroanal. Chem.*, 170 (1984) 99.
- [42] M. Penczek, Z. Stojek, *J. Electroanal. Chem.*, 181 (1984) 83.
- [43] M. Penczek, Z. Stojek, *J. Electroanal. Chem.*, 227 (1987) 271.
- [44] A. Constantinides, "Applied numerical methods with personal computers", McGraw-Hill, 1987, New York.
- [45] S.D. Conte, C. de Boor, "Elementary numerical analysis", 2ª Ed., McGraw-Hill Kogakusha, 1972, Tokyo
- [46] M.A.N.D.A. Lemos, A.J.L. Pombeiro, *J. Organomet. Chem.*, 438 (1992) 159.
- [47] A.J.L. Pombeiro, M.A.N.D.A. Lemos, M.F.N.N. Carvalho, "Actas do IX Congresso Iberoamericano de Electroquímica", Canárias, 1990, 4-12, p. 453.
- [48] A.J.L. Pombeiro, "Chemistry and Electrochemistry of Alkyne- and Isocyanide-Derived Carbyne Complexes of Rhenium, Molybdenum and Tungsten", in "Transition Metal Carbyne Complexes", (NATO Advanced Research Workshop), F.R. Kreissl (Ed.), NATO ASI Series, Kluwer Academic Publishers, Dordrecht, The Netherlands, 1993, p. 105-121.
- [49] M.A.N.D.A. Lemos, M.F.C. Guedes da Silva, A.J.L. Pombeiro, *Inorg. Chim. Acta*, 226 (1994) 9.